International Journal of Biological Macromolecules 262 (2024) 129781

Contents lists available at ScienceDirect

International Journal of Biological Macromolecules

journal homepage: www.elsevier.com/locate/ijbiomac

Three-dimensional solution structure, dynamics and binding of thioredoxin *m* from *Pisum sativum*☆

José L. Neira [a,b,*], Martina Palomino-Schätzlein [c], Virginia Rejas [d], José A. Traverso [e], Manual Rico [f,1], Julio López-Gorgé [g,1], Ana Chueca [g], Ana Cámara-Artigas [h]

[a] IDIBE, Universidad Miguel Hernández, 03202 Elche, Alicante, Spain
[b] Instituto de Biocomputación y Física de Sistemas Complejos (BIFI), Universidad de Zaragoza, 50018 Zaragoza, Spain
[c] ProtoQSAR SL, CEEI-Valencia. Parque Tecnológico de Valencia, Av. Benjamin Franklin 12 (Dep. 8), 46980 Paterna, Valencia, Spain
[d] Centro de Investigación Príncipe Felipe, Calle de Eduardo Primo Yufera 3, 46012, Valencia, Spain
[e] Department of Cell Biology, Faculty of Science, University of Granada, 18001 Granada, Spain
[f] Instituto de Quimica Física Blas Cabrera (CSIC), Calle Serrano 119, 28006 Madrid, Spain
[g] Departamento de Bioquímica, Biología Celular y Molecular de Plantas, Estación Experimental Zaidin, Consejo Superior de Investigaciones Científicas (CSIC), Prof. Albareda 1, 18008 Granada, Spain
[h] Departamento de Química y Física, Research Center CIAIMBITAL, Universidad de Almería- ceiA3, 04120 Almería, Spain

ARTICLE INFO

Keywords:
Thioredoxin
Protein-protein interactions
NMR
Fluorescence
Fructose-1,6-bisphosphatase
Peptide

ABSTRACT

Thioredoxins (TRXs) are ubiquitous small, globular proteins involved in cell redox processes. In this work, we report the solution structure of TRX m from *Pisum sativum (pea)*, which has been determined on the basis of 1444 nuclear Overhauser effect- (NOE-) derived distance constraints. The average pairwise root-mean-square deviation (RMSD) for the 20 best structures for the backbone residues (Val7-Glu102) was 1.42 ± 0.15 Å, and 1.97 ± 0.15 Å when all heavy atoms were considered. The structure corresponds to the typical fold of TRXs, with a central five-stranded β-sheet flanked by four α-helices. Some residues had an important exchange dynamic contribution: those around the active site; at the C terminus of β-strand 3; and in the loop preceding α-helix 4. Smaller NOE values were observed at the N and C-terminal residues forming the elements of the secondary structure or, alternatively, in the residues belonging to the loops between those elements. A peptide derived from pea fructose-1,6-biphosphatase (FBPase), comprising the preceding region to the regulatory sequence of FBPase (residues Glu152 to Gln179), was bound to TRX m with an affinity in the low micromolar range, as measured by fluorescence and NMR titration experiments. Upon peptide addition, the intensities of the cross-peaks of all the residues of TRX m were affected, as shown by NMR. The value of the dissociation constant of the peptide from TRX m was larger than that of the intact FBPase, indicating that there are additional factors in other regions of the polypeptide chain of the latter protein affecting the binding to thioredoxin.

1. Introduction

Thioredoxins (TRXs) are a family of small, globular proteins (~10–13 kDa) present in all living systems from eukaryotic to prokaryotic cells [1–4], but plants exhibit the most complex TRX multigenic family, as shown by the analyses performed in Arabidopsis and rice genomes [5]: for instance, the *Arabidopsis thaliana* genome encodes >25 different TRXs and other TRX-like proteins with several TRX domains [6]. TRXs are heat-stable proteins with an acidic isoelectric point, working as disulfide oxido-reductase enzymes, with a well-known scaffolding: a five-stranded β-sheet, sandwiched by four α-helices: a βαβαβαββα. This fold has been identified in numerous proteins, including glutaredoxins [7], glutathione-S-transferase [8], protein disulfide isomerase [9] and Dsb proteins from *E. coli* periplasm [10]. Their catalytic mechanism involves, in most of the examples described so far, a conserved pentapeptide sequence: WC(G/P)PC motif [11,12]; this motif remains unaltered in all the TRX protein sequences reported to date, regardless of the residue variation in the rest of the sequences. The active site cysteines of TRXs are oxidized, reducing other proteins, through a

☆ This paper is dedicated to the memory of Manuel Rico (a mentor, colleague and friend) and Julio López-Gorge (a mentor, friend, colleague and husband).

* Corresponding author at: IDIBE, Edificio Torregaitán, Universidad Miguel Hernández, Avda. del Ferrocarril s/n, 03202 Elche, Alicante, Spain.
E-mail address: jlneira@umh.es (J.L. Neira).

[1] Deceased.

https://doi.org/10.1016/j.ijbiomac.2024.129781
Received 14 December 2023; Received in revised form 23 January 2024; Accepted 24 January 2024
Available online 1 February 2024

Abbreviations

CD	circular dichroism
FBPase	fructose-1,6-bisphosphatase
FBPpep	fragment derived from FBPase, with the sequence E^{152}SLPDYGDDSDDNTLGTEEQRSIVNVSQ^{179}
Fd	ferredoxin
HSQC	heteronuclear single quantum coherence
IPTG	isopropyl-β-D-1-thiogalactopyranoside
NMR	nuclear magnetic resonance
NOE	nuclear Overhauser enhancement
NADP	nicotinamide adenine dinucleotide phosphate
NADPH	reduced nicotinamide-adenine dinucleotide-phosphate
NOESY	2D nuclear Overhauser enhancement spectroscopy
RMSD	root-mean-square deviation
TOCSY	2D total correlation spectroscopy
TPPI	time proportional phase increment
TRX	thioredoxin
TSP	3-(trimethylsilyl) propionic acid-2,2,3,3-$^{2}H_4$-sodium salt
UV	ultraviolet

reversible disulfide-dithiol reaction of the two SH groups [1]; in fact, the reduced TRXs are the major cellular protein disulfide reductases in living organisms, and they also work as an electron donor for particular enzymes of primary metabolism. The reaction mechanism of TRXs involves a nucleophilic attack on one of the cysteines in a target protein by the catalytic cysteine in the TRX redox-active motif, forming an intermolecular disulfide between TRX and the target protein. This intermolecular disulfide bond is reduced, resulting in the reduced target protein and oxidized TRX. The oxidized TRX is reactivated through reduction by a specific enzyme called thioredoxin reductase [13,14] (in fact, both proteins form the so-called thioredoxin system). Therefore, TRXs are capable of interacting with other targets, having a crucial role in many cellular redox metabolism processes, activation of transcription factors, regulation of photosynthetic events in plants, and in regulation pathways in other species such as cell proliferation, insulin degradation, blood clotting, seed germination and repair of oxidative damage [11,15–19] (Fig. 1). As a consequence, in animals TRXs are associated with cancer, cardiac disease or viral infections [20,21]; furthermore, recently, TRXs have been used as potential therapeutic regulators of cell growth, apoptosis and inflammation [16,22] (Fig. 1).

Based on their gene sequences, there are two families of TRXs: family I includes proteins with a single TRX domain, whereas family II is composed of multiple TRX-like domains. At least twenty TRX-encoding genes belonging to family I have been reported in *Arabidopsis thaliana*, while in mammals (humans included) there are only two, as well as in *E. coli* [23–25]: TRX1 (TXN1 in humans) and TRX2 (TXN2). Whereas the protein codified by TRX2 is mitochondrial, that from TRX1 appears to be cytosolic (but it is also present in the nucleus and at another cell locations). In plant chloroplasts, two TRX systems are present with different sources of reducing power. In the first system, ferredoxin (Fd)-thioredoxin reductase (FTR) is involved in the Fd-TRX system, and it activates the chloroplasts TRXs by reducing equivalents from photosynthetically reduced (activated) Fd [26–28]. The second system is the reduced nicotinamide-adenine dinucleotide-phosphate (NADPH)-dependent chloroplast thioredoxin reductase that is reduced by NADPH, present in chloroplasts. The chloroplasts contain multiple types of TRXs: two TRX f; four TRX m; and two y isoforms, as well as x- and z-type of TRX [29–31]. TRXs also intervene in plastid transcription, ATP synthesis, chloroplast biogenesis, carbon, nitrogen and sulfur metabolism, chloroplast biogenesis and oxidative stress responses [27,32] (Fig. 1). Due to that plethora of functions, some of the plastid TRXs are involved in regulation of several enzymes [11,28,33]: for instance, TRX m activates the nicotinamide-adenine dinucleotide-phosphate- (NADP) dependent malate dehydrogenase [33] and TRX f activates the fructose-1,6-bisphosphatase (FBPase), among other Calvin cycle enzymes [11,26,33,34]. However, it has been shown that TRX m also activates chloroplast FBPase [35–38] [39]. FBPpase catalyzes the breakdown of fructose-1,6-bisphosphate to fructose-6-phosphate and phosphorous; this reaction has a large free energy change and it is a regulatory step for pathways where FBPase intervenes. In general, FBPase activity is regulated by electron availability through a modulating mechanism involving the Fd-thioredoxin system [26,40–42]. Our groups have shown that the preceding region of the FBPase regulatory sequence, comprising residues Leu154 to Glu170 is the thioredoxin docking site [38,40,42,43]. Therefore, we wondered whether such isolated region

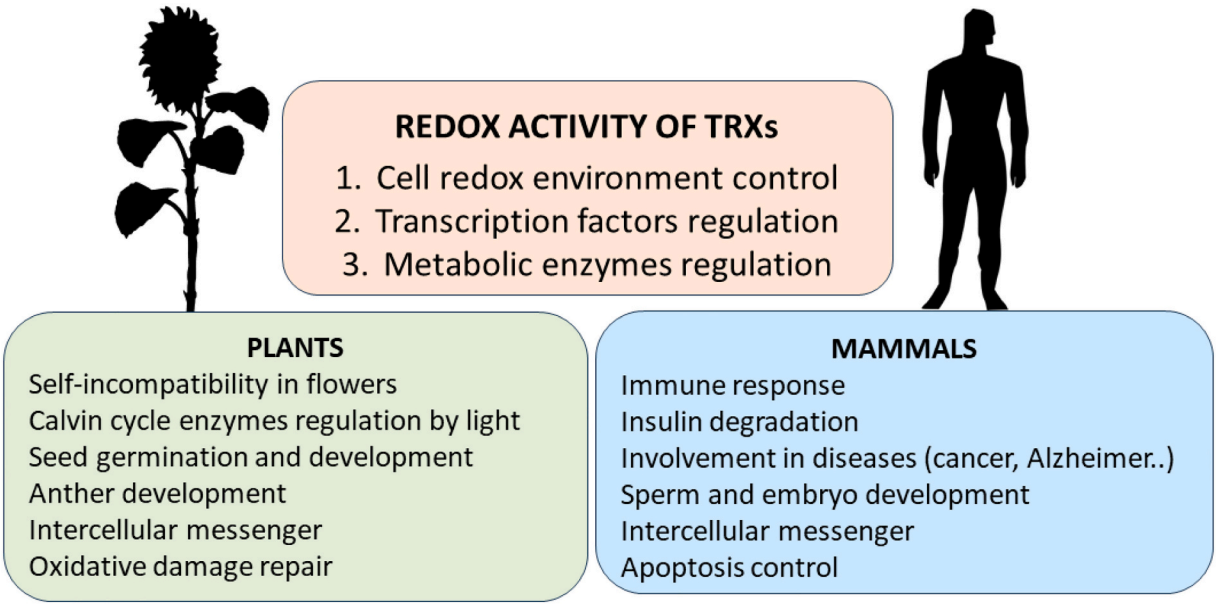

Fig. 1. Functions of thioredoxins: Scheme showing some well-established roles for plant (left-hand-side figure) and mammals (right-hand-side figure) thioredoxins (TRXs) based on their molecular redox activity (centered figure).

could be capable of binding to the intact TRX m, and if so whether the measured affinity was similar to that of the intact FBPase. If the TRX-peptide affinity was similar to that of TRX-FBPase, we could modulate the binding between the two proteins with such peptide.

In this work, we report the ^{15}N, ^{13}C and ^{1}H assignments of TRX m (108 residues) from *Pisum sativum* (pea), its three-dimensional solution structure, its dynamics in the ns-ps time regime, and its binding to a peptide derived from FBPase, comprising the TRX-binding site of the intact protein (residues Glu152 to Gln179) [38,39,43]. The obtained structure was similar to that of TRX m from spinach [44], adopting the TRX fold, with minor differences in the length of some of the strands comprising the β-sheet and some of the helices: namely, a five-stranded β-sheet, sandwiched by four α-helices, located at the external side of the β-sheet, with a general βαβαβαββα scaffolding. The active-site center (preceding the second α-helix); the C terminus of β-strand 3; and the C-terminal segment (comprising the last fourth α-helix) appeared to be highly mobile. Binding of the peptide derived from the pea FBPase, containing the thioredoxin docking site, occurred with a dissociation constant, K_d of ~2 μM, as determined by fluorescence, and K_d of ~50 μM, as determined from NMR titrations (followed by 2D ^{15}N, ^{1}H-HSQC spectra). However, this value differed from that of the intact FBPase (0.019 μM), obtained by a Koshland-Nemethy-Filmer model [39], indicating the TRX cooperative binding to the FBPase. In our case, probably, the isolated nature of the pea FBPase peptide showed only the energetics of the interactions (and, probably, folding) of the peptide in its binding site on the TRXs, without any cooperativity effect. Therefore, our results show that other factors in the polypeptide chain of TRX might intervene in the binding to FBPase.

2. Materials and methods

2.1. Materials

Imidazole, Trizma base, DNase, SIGMAFAST protease tablets, deuterium oxide (99 % atom in $^{2}H_2O$), NaCl, Ni^{2+}-resin, 3-(trimethylsilyl) propionic acid-2,2,3,3-$^{2}H_4$-sodium salt (TSP), DTT (dithiothreitol) and Amicon centrifugal devices with a molecular weight cut-off of 3 kDa were from Sigma (Madrid, Spain). The β-mercaptoethanol was from BioRad (Madrid, Spain). Kanamycin and isopropyl-β-D-1-thiogalactopyranoside (IPTG) were obtained from Apollo Scientific (Stockport, UK). Triton X-100, Tris(2-carboxyethyl)phosphine (TCEP), dialysis tubing with a molecular weight cut-off of 3500 Da, and the SDS protein marker (PAGEmark Tricolor) were from VWR (Barcelona, Spain). The rest of the materials were of analytical grade. Water was deionized and purified on a Millipore system.

2.2. TRX m cloning, expression and purification

The cDNA from TRX m from *Pisum sativum* [37] was subcloned using BamHI and *Hin*dIII restriction sites into pETM11 plasmid (Novagen), and modified to yield a protease cleavable N-terminal hexahistidine (His_6)-tag. The thrombin cleavage sequence is formed by –GLVPRGSH–, where the protease cleaves between the R and G residues. The cloned protein had a K at position 87 instead of an R, as the originally deposited pea TRX m in UniProt. Plasmid encoding the (His_6)-tagged protein was introduced into competent *E. coli* BL21 (Merck, Madrid, Spain) cells. Transformed cells were grown at 37 °C of LB media (containing 30 mg/mL kanamycin) until an OD_{600} of 0.6–0.9 was reached. The expression in M9 minimal media was supplemented with 1 g/L of $^{15}NH_4Cl$ for ^{15}N-labelled samples, or, alternatively for double labelled samples used in TRX m assignment, with 1 g/L of $^{15}NH_4Cl$ and 2 g/L of ^{13}C-glucose. The addition of a final concentration of 1 mM IPTG (1 mL of a stock solution 1 M IPTG to 1 L of media) when the above indicated OD_{600} was reached, induced protein expression either in LB or in M9 minimal media. After adding IPTG, the cells were incubated overnight at 37 °C and harvested by centrifugation.

Protein (either in LB or minimal media) was purified by Ni^{2+}-affinity chromatography in a prepacked HiTrap affinity column (GE Healthcare, Barcelona, Spain) according to the manufacturer's indications. Briefly, cell pellets were resuspended in 50 mL containing 50 mM Tris (pH 8.0), 1 % Triton X-100, 0.5 M NaCl, 1 mM β-mercaptoethanol and 10 mM imidazole (buffer A) with 1 % Triton X-100 and a single SIGMAFAST tablet. The suspension of the cells was lysed by sonication on ice with 10 bursts of 45 s at maximum power interleaved with 15 s keeping in ice (the sonicator was a Branson model 102C). Insoluble cell debris was removed from the cell lysate by centrifugation. The supernatant was loaded onto the HiTrap affinity column, equilibrated with buffer A. The protein was eluted with a linear gradient of buffer B (buffer A + 1 M imidazole). Fractions containing the target protein were pooled together, concentrated by using Amicon centrifugal devices, and loaded onto a Superdex 75 16/60 size-exclusion column (GE Healthcare) equilibrated with 25 mM phosphate buffer (pH 7.0) with 150 mM NaCl, on an AKTA FPLC (GE Healthcare) by following the absorbance at 280 nm. The (His_6)-tag was cleaved off by using commercial thrombin (GE Healthcare) as described previously [45,46]. After cleavage, the protein had the additional residues at its N terminus: GSHM–. The concentration of pure protein was determined by measuring the absorbance at 280 nm with the extinction coefficients as determined by the sequence [47].

2.3. Peptide design

Peptide was synthesized and purified by GenScript (Amsterdam, Netherlands) with a purity larger than 98 %; purity was checked by mass spectrometry, and by SDS-PAGE in our own laboratory. The sequence of the peptide (FBPpep), coming from the pea fructose-1,6-bisphosphatase, was E^{152}SLPDYGDDSDDNTLGTEEQRSIVNVSQ^{179}, with the C terminus amidated. The following residues of the original FBPase sequence: (a) Cys153, Cys173 and Cys178 were mutated to serine to avoid the formation of intra- or inter-disulfide bridges; and (b) Phe157 was mutated to tyrosine to allow for reliable absorbance detection of the peptide at 280 nm [47]. In the crystal structure of oxidized pea FBP, Cys153 and Cys173 form a disulfide bond [48], but in the structure of the C153S mutant the secondary structure is conserved independently of the disulfide bridge formation. Although this mutation affects the redox-dependent regulation of the enzyme [49], since we are going to measure binding, and not the redox properties of the peptide, we decided to work with the peptide where the three cysteines where mutated to serine to avoid peptide aggregation by intermolecular cysteine oxidation.

2.4. Fluorescence binding experiments

Fluorescence spectra were collected on a Cary Varian spectrofluorometer (Agilent, Santa Clara, CA, USA), interfaced with a Peltier unit. A 1-cm-pathlength quartz cell (Hellma, Kruibeke, Belgium) was used. Excitation and emission slit widths were set to 5 nm. Voltage of the photomultiplier was set to 650 V. Data were collected every 1 nm. For the titration between FBPpep and TRX m, increasing amounts of FBPpep, in the concentration range 0–10 μM (final concentration), were added to a solution with a fixed concentration of TRX m (1.9 μM) in the presence of DTT (1 mM). The samples were prepared the day before and left overnight at 5 °C; before the measurements, they were incubated for 1 h at 30 °C. Experiments were carried out in phosphate buffer (50 mM), pH 5.8 at 30 °C. The samples were excited at 280 and 295 nm. In all cases, the appropriate blank-corrections were made by subtracting the signal obtained with the corresponding amount of FBPpep with KaleidaGraph (Synergy software, Reading, PA, USA). Spectra were corrected for inner-filter effects during fluorescence excitation [50]. The titration was repeated three times, using new samples; variations in the results among the three experiments were lower than 10 %.

The dissociation constant of the complex, K_d, was calculated by fitting the binding isotherm constructed by plotting the observed fluorescence change as a function of FBPpep concentration to the general

binding model, explicitly considering protein depletion due to binding [51,52]:

$$F = F_0 + \frac{\Delta F_{max}}{2[\text{TRX m}]_T}\left([\text{FBPpep}]_T + [\text{TRX m}]_T + K_d\right) - \sqrt{\left(\left([\text{FBPpep}]_T + [\text{TRX m}]_T + K_d\right)^2 - 4[\text{FBPpep}]_T[\text{TRX m}]_T\right)}, \quad (1)$$

where F is the measured fluorescence at any particular concentration of FBPpep after subtraction of the spectrum of the sample containing only the same concentration of such polypeptide (i.e., F is the differential, or difference fluorescence); ΔF_{max} is the largest change in the fluorescence of FBPpep when all polypeptide molecules were forming the complex, compared to the fluorescence of each isolated protein (at the same corresponding concentration); F_0 is the fluorescence intensity when no FBPpep was added; $[\text{TRX m}]_T$ is the constant, total concentration of TRX m (1.9 μM); and $[\text{FBPpep}]_T$ is that of FBPpep, which was varied during the titration. Fitting to Eq. (1) was carried out by using KaleidaGraph.

2.5. Circular dichroism (CD)

Far-UV CD spectra of FBBpep were collected on a Jasco J810 spectropolarimeter (Jasco, Tokyo, Japan) with a thermostated cell holder and interfaced with a Peltier unit at 5 °C. The instrument was periodically calibrated with (+)-10-camphorsulfonic acid. A cell of path length of 0.1 cm was used (Hellma, Kruibeke, Belgium). All spectra were corrected by subtracting the corresponding baseline obtained from the spectrum of a solution containing only the buffer with KaleidaGraph. The buffer was the same used in the fluorescence titration experiments. Isothermal wavelength spectrum of FBPpep was acquired as an average of 6 scans, at a scan speed of 50 nm/min, with a response time of 2 s and a band-width of 1 nm.

2.6. Nuclear magnetic resonance (NMR)

NMR samples for homonuclear experiments were prepared by concentrating and exchanging the solution containing the TRX m obtained from the gel filtration purification step in Amicon 3 K centrifugal devices, in a final 9:1 H_2O:^2H_2O solution, with a 0.02 % NaN_3 in phosphate buffer (50 mM), pH 5.8. The solution was centrifuged briefly to remove insoluble protein and then transferred to a 5 mm NMR tube. Spectra were recorded on a Bruker Avance 500 MHz spectrometer (Bruker GmbH, Karlsruhe, Germany), with z-pulse field gradients and a TXI probe, equipped with Topspin 2.1 software (Bruker, Karlsruhe, Germany). Experiments were run at 30 °C; the temperature of the probe was calibrated with methanol [53]. The pH of the solution was measured at the beginning and end of the complete series of experiments by using a Russell glass electrode, without finding any difference between both measurements. Values of the pH reported here represent apparent values of pH, without correction for isotope effects. TSP was used as the internal chemical shift reference and corrected for the pH value in all spectra described below [53].

The NMR experiments with $^{13}C/^{15}N$-labelled TRX m samples were performed in the same magnet with the same buffer (and 1 mM DTT), and at the same temperature as the homonuclear experiments by using Amicon 3 K centrifugal devices to concentrate the sample, in a final 9:1 H_2O:^2H_2O solution, with a 0.02 % NaN_3 in phosphate buffer (50 mM), pH 5.8. Thus, we were determining the structure of the reduced protein, as we ran the experiments in the presence of a reducing agent; this redox agent should avoid the problems of having some population of the oxidized state, due to the oxygen dissolved in the solution. Protein concentration was 2.5 mM for either double labelled or unlabelled samples.

(a) Assignment of TRX m: The NMR experiments used for sequence specific assignment of HN, N, C_α and C_β resonances of a $^{13}C/^{15}N$-labelled TRX m were HNCACB, HNCA, HNCO, HCCCONH [53]. Standard 2D NOESY (mixing time 90 ms) and 2D TOCSY (mixing time, 80 ms) homonuclear experiments spectra were also run to allow for identification of additional protons in the side-chain of residues and for finding NOE restrictions [54,55]. The details of the acquisition parameters of all the experiments used are shown in Supplementary Table 1 (Table ST1). The chemical shifts have been deposited in the BMRB (Biomagnetic Resonance Bank) with number 52150. The 2D ^{15}N-HSQC spectra were also acquired in the TPPI (time proportional phase increment) mode at the beginning, in-between and at the end of the triple-resonance suite of experiments to ensure sample integrity during the long acquisition times. Processing and analysis of data was carried out by using the Bruker software (Topspin 2.1).

(b) Relaxation measurements of TRX m: We ran ^{15}N-R_1,^{15}N-R_2 and ^1H—^{15}N NOE experiments. All the relaxation measurements were determined in an interleaved manner to ensure that the experimental conditions were the same for the different relaxation delays. The temperature was the same used in the assignment (30 °C). All experiments were acquired by using gradient pulse sequences developed by Kay and co-workers [56]. The T_1 (=1/R_1) relaxation time was measured with typically 10 inversion-recovery delays, varying from 5 to 650 ms; T_2 (=1/R_2) was determined by collecting 8 time points ranging from 50 to 400 ms. Two relaxation delays were randomly repeated in each series of rates to ensure reproducibility. For the T_1 and T_2 pulse sequences, the delay between scans was 5 s. Cross-peaks intensities at each time were measured by integration of signals in Topspin 2.1. Intensity variation in the T_1 and T_2 experiments of each cross-peak was fitted to simple exponential functions, with a pre-exponential factor by using KaleidaGraph. Errors shown in the T_1 and T_2 were from fitting errors.

The ^1H—^{15}N NOE experiment was measured by recording interleaved spectra with or without proton saturation. The ^1H—^{15}N NOE spectrum recorded in the presence of proton saturation was acquired with a saturation time of 10 s. The ^1H—^{15}N NOE spectrum recorded without proton saturation incorporated a relaxation delay of 10 s. The ^1H—^{15}N NOE experiment (with and without saturation) was repeated twice. The NOE ratio was defined as NOE = I_{sat}/I_{ref}, where I_{sat} is the intensity of the corresponding cross-peak in the saturated spectrum and I_{ref} is that in the reference (non-saturated) spectrum. The intensities of the cross-peaks in both spectra were measured by using Topspin 2.1. Errors in the NOEs were estimated to be 10 % as judged from the integrated regions where no peaks were observed.

Spectra were recorded with 2048 × 180 complex matrices in the F_2 and F_1 dimensions, respectively, with typically 32 scans (NOE experiment) and 16 scans (R_1 and R_2 experiments) *per* F_1 experiment. Spectral widths of 1935 and 7000 Hz were used in F_1 and F_2 dimensions, respectively; the ^{15}N carrier was set at 120 ppm and that of ^1H was set on the water signal in all the experiments.

(c) Assignment of FBPpep: Two-dimensional homonuclear spectra of the peptide were acquired in each dimension in phase-sensitive mode by using the TPPI technique [57] and a spectral width of 5500 Hz in both dimensions. Peptide concentration was 2.0 mM, and the temperature was 5 °C; the pH was 5.8, phosphate buffer (50 mM). Standard 2D TOCSY [58] and NOESY [59] (with mixing times of 80 and 250 ms, respectively) were performed by acquiring a data matrix size of 2048 × 256 points. The relaxation time in both experiments was 1 s. The DIPSI (decoupling in the presence of scalar interactions) spin-lock sequence [60] was used in the TOCSY experiments. A number of 88 scans were acquired *per* increment in the first dimension, and the residual water signal was removed by using the WATERGATE sequence [61]. NOESY spectra were collected with 128 scans per increment in the first dimension, using again the WATERGATE sequence [61]. In both spectra, data were zero-filled, resolution-enhanced with a square sine-bell window function optimized in each spectrum, baseline-corrected and processed with Topspin 2.1. The ^1H resonances were assigned by standard sequential assignment processes [53]. The chemical shift values of H_α protons in random-coil regions were obtained from tabulated data, corrected by neighboring residue effects [53,62–64]. Spectra were

referenced with internal TSP considering the pH-dependence of the methyl signal [53].

(d) Temperature coefficients of FBPpep: The chemical shifts of the amide protons usually exhibit a linear dependence with temperature, whose slope is referred to as "temperature coefficient". The temperature coefficients ($\Delta\delta/\Delta T$) for solvent-accessible amide protons are in the range − 6 to −10 ppb K^{-1}. Temperature coefficients small in absolute values (i.e., $|\Delta\delta/\Delta T| \leq 4.0$ ppb K^{-1}) are indicators of solvent inaccessibility, suggesting that the corresponding amide protons are probably involved in hydrogen-bonds [65–67]. We measured the temperature coefficients of the amide protons of FBPpep by acquiring TOCSY experiments at 5, 10, 15 and 17 °C at the same pH described above. The TOCSY experiments were referenced by using TSP, considering the pH-dependence of the methyl signal [53].

(e) Titration of FBPpep over TRX m followed by NMR: The cross-peaks in the 2D $^{1}H,^{15}N$ HSQC NMR spectra [68] of TRX m, at different FBPpep concentrations, were identified by using the assignment provided in this work. Spectra were acquired in the TPPI mode at 25 °C (the temperature was chosen to allow for comparison with the titration fluorescence experiments), in phosphate buffer (50 mM), pH 5.8 in the presence of 1 mM DTT. The concentration of ^{15}N-labelled TRX m was 70 μM either in isolation or in the presence of increasing concentrations of FBPpep (from 0 to 943 μM, final concentration). The spectra were typically acquired with 2048 complex points in the ^{1}H dimension, 200 complex points in the ^{15}N dimension, with 192 scans. Typical spectral widths for the 2D $^{1}H—^{15}N$ HSQC spectra were 6000 (^{1}H) and 1500 (^{15}N) Hz. Water was removed by using the WATERGATE sequence [61]. After the acquisition of each experiment, at a particular peptide concentration, the sample was lyophilized and the corresponding amount of a FBPpep stock solution (2 mM) was added to the dried powder to yield the next peptide concentration. It could be thought that this procedure of lyophilization after the acquisition of each titration point could result in artifacts and they would be responsible for the behavior observed in the intensities of the cross-peaks of the protein (Section 3.3.2), as the peptide concentration was raised. Control experiments carried out with samples of ^{15}N-TRX m concentrated by using lyophilization or Amicon-concentration devices yielded similar 2D $^{1}H—^{15}N$ HSQC spectra, with no variations in the signal intensity (volume). Besides, it is quite unlikely that any artifact associated with lyophilization would result in a decrease of intensities in a sigmoidal-like way.

The resulting matrix of each experiment was zero-filled to double the number of original points in all dimensions, and shifted squared sine-bell apodization functions were applied before Fourier transformation. NMR data were processed and analyzed using TopSpin 2.1. Cross-peaks intensities (volumes) were corrected by the corresponding value of the receiver gain for each experiment. All the 2D $^{1}H,^{15}N$ HSQC NMR spectra were referenced with the methyl protons of external TSP for ^{1}H and for the indirect ^{15}N dimension [53].

The variations in the intensities of the cross-peaks of 2D $^{1}H,^{15}N$ HSQC NMR spectra of TRX m, corrected by the corresponding receiver gain, were fitted to:

$$F = F_0 + \frac{\left(\Delta F_{max}\,[\mathrm{FBPpep}]_T\right)}{\left([\mathrm{FBPpep}]_T + K_d\right)} \quad (2),$$

which is a simplified expression of Eq. (1). The meanings of all symbols are the same as those previously indicated in Eq. (1).

2.7. Structure calculations

All spectra were analyzed manually by using the Sparky software [69]. After integration, the peak volumes and chemical shifts list were output to a CYANA 2.1.-compatible format [70–72]. The automatic calibration method implemented in CYANA, CALIBA [72], was run to transform the peak volumes into distances. The upper limits obtained were used without modification for the initial structure calculations.

Structures of TRX m were calculated by using the NOE distance restraints with the program CYANA. This was an iterative process because many chemical shifts of TRX m could be assigned to more than a single nucleus, and therefore, many NOE cross-peaks were ambiguous, meaning that a cross-peak in the NOESY spectrum many times could be assigned to a set of possible pairs of protons [73,74]. At subsequent steps during the calculation of the structures, those distance restraints were combined in an iterative fashion with: (i) backbone ϕ and ψ angle restraints as predicted by TALOS+ [75] based on the chemical shifts of C_α, C_β, H_α, H_β, NH, amide N and CO atoms (only when angular predictions were classified as "good" were used in the calculations); and (ii) hydrogen-bonds obtained from the remaining amide protons observed in hydrogen-exchange experiments carried out by dissolving the protein in 99.99 % D_2O, at 0.2 mM final concentration, and acquiring a short 2D $^{1}H—^{15}N$ HSQC NMR spectrum. The introduced hydrogen-bond restraints were in all cases well-suited with the observed, experimental distance restraints from NOESY spectra, and they were only introduced as restraints, when the first runs of CYANA, predicted the presence of such hydrogen bonds in at least 15 of the best 20 conformers (with the lowest target functions). Each hydrogen-bond was specified by two distance restraints: HN-O distance of 1.7–2.3 Å and N—O distance of 2.4–3.3 Å [73,74,76].

The resulting initial structures, obtained with CYANA (without the addition of hydrogen-bonds as restrictions), and which had the lowest target functions in the ensemble of conformers, were used to assign additional, ambiguous peaks (because either they were mis-assigned or there was chemical shift overlapping) in the NOESY spectrum. It is important to stress out that we did not use all the NOEs from the NOESY spectrum at the first calculations, but only those which had been unambiguously assigned. The quality of the introduced constraints was checked at every step by analyzing the restraint violations of the calculated conformers. The NOE cross-peaks corresponding to restraints that were consistently violated in a significant number of structures were checked for possible overlapping in the NOESY spectra and the corresponding restraints were modified. The cycle was repeated until no consistent violation was detected. The cycle of calculations and assignments was repeated until no further assignments were possible.

A total of 300 random conformers were annealed in 12,000 steps. The 20 conformers with the lowest target function constituted the final family of structures of TRX m. The quality of the structures was evaluated in terms of deviations from ideal bond lengths, angles, and through Ramachandran plots by using the PSVS server [77].

3. Results

3.1. Description of the structure of TRX m from pea

Several repeated rounds of ambiguous long-range and non-sequential NOEs were assigned, with the help of the first structures, obtained from the calculations, with the lowest target function, and converted to distance constraints to be used as input data in CYANA, together with the previously unambiguously assigned NOEs. We also removed restraints that were repeatedly violated in the structure calculations. Table 1 summarizes the number of structurally relevant intra-residual, sequential, medium- and long-range constraints used in the calculations. The RMSD values for all backbone atoms and heavy atoms between residues Val7 and Glu102 were 1.42 ± 0.15 Å and 1.97 ± 0.15 Å, respectively. The target function of CYANA had an average value of 0.51 ± 0.12 (in the range 0.30 to 0.70). These values of the RMSD among the conformers were similar to those of other solution structures of TRXs from other species (see for instance [78]). There were no distances smaller than 2.2 Å for heavy atoms, nor distances smaller than 1.6 Å for hydrogens. The RMSD for covalent bonds relative to the standard value was 0.001 Å, and that for covalent angles was 0.2 degrees, as indicated by the PSVS web-server [77].

The overall fold of TRX m from pea indicates a core formed by a five-

Table 1
NMR restraints and structural statistics for the best 20 structures.

Restraints	
Total number of restraints	
NOE restraints[a]	1444
Intra-residue (i-j = 0)	446
Sequential (|i-j| = 1)	400
Medium-range (|i-j| ≤ 4)	238
Long-range (|i-j| ≥ 4)	360
Dihedral angle restraints	114 (for ϕ and ψ angles)
Hydrogen-bond restraints	29 x 2[b]
RMSD to the mean structure residues Val7-Glu102 (in Å)	
Average backbone	1.42 ± 0.15
Heavy atoms	1.97 ± 0.15
Ramachandran summary for all residues in the 20 conformers from Procheck (in %)[c]	
Most favored	52.2
Additionally allowed regions	33.3
Generously allowed regions	10.5
Disallowed regions	4.1

[a] The i and j represent two residues of the sequence of TRX m.
[b] For each hydrogen-bond two restrictions were introduced: the HN-O and the N—O distances.
[c] Obtained from PSVS server [77].

stranded mixed β-sheet, surrounded by four α-helices (Fig. 2). The α1 and α3 helices pack on one side of the β-sheet. Conversely, the α2 and α4 helices pack on the other side of the β-sheet, as judged by the proximity of several of the side-chains of their residues, as concluded from the NOEs between the side-chains of Leu46 and Lys103, or between Tyr50 and Glu105, among others. However, these interactions do not prevent the fraying of α4, as it has been observed in the structure of TRX m from spinach [44]. The scaffolding of β-sheets and α-helices is similar to those observed in other TRXs (see [44,79] and references therein), but some of the latter were shorter and more irregular in the TRX m from pea (see below). In the TRX m from spinach, the Pro77 is in a cis conformation; however, we could not detect any NOE between the H_α proton of Ile76 (at 4.65 ppm) and the H_α proton of Pro77 (at 5.17 ppm) because of proximity to residual water signal; then, during the calculations Pro77 adopted a trans conformation in TRX m from pea.

The use of the chemical shifts of $^{13}C_\alpha$, $^{13}C_\beta$, ^{13}CO, H_α, H_β, NH and amide ^{15}N atoms in TALOS+ [75] predicted the following elements of secondary structure: a five-stranded pleated β-sheet, which is twisted, and composed of parallel (p) and antiparallel (a) strands following the arrangement: Gln6-Val8 (β-strand 1 p); Ile54-Leu59 (β-strand 3 p); Val24-Trp29 (β-strand 2 p); Pro77-Lys83 (β-strand 4 a); and Ser90-Ile92 (β-strand 5 a). The presence of these strands was confirmed by: (i) long-distance NOEs involving backbone amides and H_α protons of residues located in the different β-strands (Fig. S1), together with long-distance NOEs of backbone amides with side-chains of residues located in the different β-strands; and, (ii) consistency between the observed slowest-exchanging protons and the hydrogen-bond scaffolding characteristic of a β-sheet conformation (Fig. 3). This five-stranded β-sheet forms the core of the molecule. The β-strand 1 did not show any solvent-exchange protected amide proton (Fig. 3), but: (i) the observed NOE between the NH of Lys58 and the H_α proton of Gln6; and, (ii) the presence of a hydrogen-bond between the NH of Val7 and the CO of Lys58 in the first obtained structures during the CYANA calculations allowed the identification of the region Gln6-Val8 as a β-strand.

The four helices were also predicted by TALOS+ software. The presence of such helices (Fig. 2) was confirmed by: (i) strong or medium NN(i,i + 1), medium αN(i,i + 2) and medium αβ(i,i + 3) NOEs (Fig. 3); and, (ii) the amide protons protected against solvent-exchange (Fig. 3). The helices were roughly spanning residues: Trp13-Leu16 (α1), Ile42-Glu49 (α2), Asn66-Lys70 (α3) and Ala98-Glu105 (α4). The four α-helices were displayed on the external surface of the globular molecule. The helices did not seem to be regular and there were deviations for the main chain torsion angles, ϕ and ψ, when compared to the standard helical values (Fig. 2). For instance, in α1, Glu15 did have both angles different to those observed in regular α-helices; in α2, Glu49 appeared to show also deviations from the ideal ϕ and ψ values, and α2, located after the active site loop, appeared to be bent; α3, where turns of a 3_{10}-helix structure were observed (hydrogen-bond scaffolding of CO(i)-NH(i + 3)), probably because the formation of a regular α-helix is hindered by Pro65; and finally, α4, with the last C-terminal residues of the helix having the largest deviations from the regular ϕ and ψ values.

The active site, involving Trp32-Cys33-Gly34-Pro35-Cys36 residues, was poorly defined; in fact, analyses of the 20 structures showed a large variation in the ϕ and ψ values, and Cys36 was among the outlier

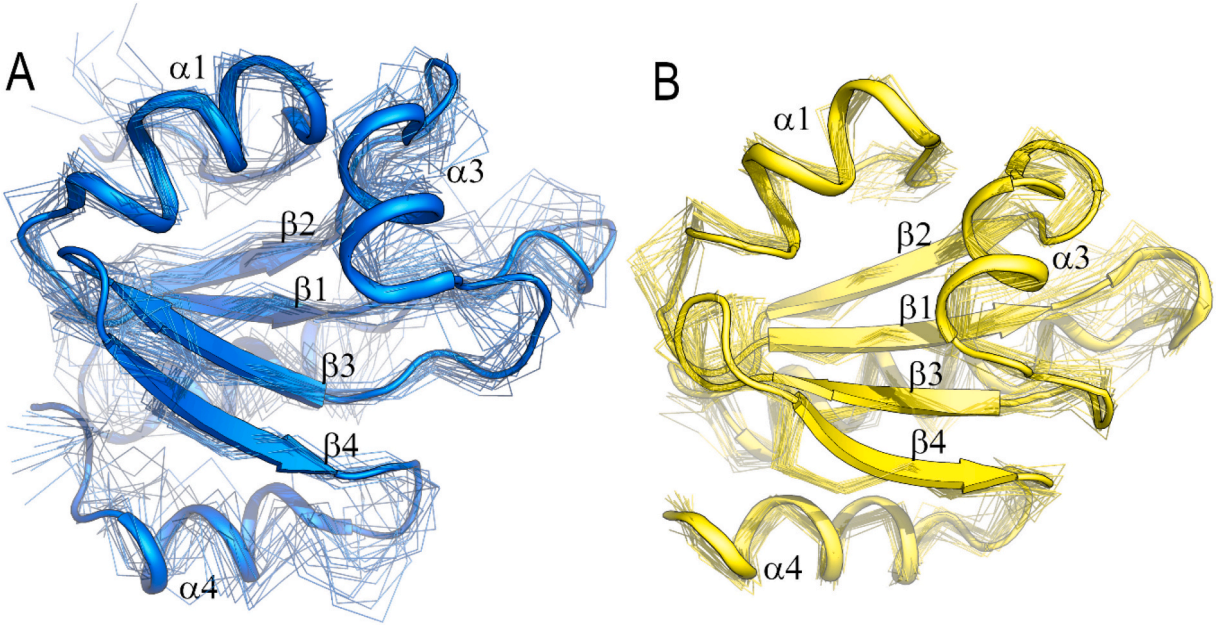

Fig. 2. Comparison of the solution structure of TRXs m from two plants. Solution structures of TRX m from pea (this work) (A) (in blue) and that of spinach (1GL8) (B) (in yellow) in the same orientation. The ribbon representation of each protein is shown together with the 20 best conformers. NMR model structures were superimposed over residues Val7-Glu102 and Val14-Leu117 for the pea and spinach enzymes, respectively. The figure was produced with PyMOL (Schrödinger).

Fig. 3. Summary of NMR data. NOEs are classified into strong, medium or weak according to the height of the bar underneath the sequence, as concluded from peak integration. Dotted bars indicate NOEs which could not be unambiguously assigned due to overlapping or proximity to the residual water signal. The corresponding sequential H_α NOE with the following H_δ of the proline residue are indicated by an open bar in the row corresponding to the αN NOEs. The white squares indicate those residues that were detected in a 2D ^{1}H,^{15}N HSQC spectrum after dissolving the sample in $^{2}H_2O$ at pH 5.8 and 30 °C; that is, they are the most solvent-exchange protected residues.

residues (together with Gln6, Ala51, Glu63, Ile76 and Ala30) in the arrangement of such angles for most of the 20 structures (the same feature happened in such active site cysteine for TRX m from spinach [44]). The active site was located at the N terminus of α2. The side-chains of the residues involved in the active site protruded from the protein surface and they did not show interactions with other protein regions, although the preceding (β-strand2) and the following (α2) polypeptide patches contact with other residues distant in the sequence. Interestingly enough, the signal of Gly34 in the 2D ^{1}H, ^{15}N-HSQC spectrum did not appear (it was possible to identify the NH in the 2D $^{1}H—^{1}H$ NOESY spectrum); the absence of the cross-peak in the ^{1}H, ^{15}N HSQC spectrum for such glycine was also reported in TRX m from spinach [44], where the residues after the last cysteine did not show any further NOE with other regions [44]. Furthermore, cross-peak broadening of all those residues close to or belonging to the active site has been also observed in the reduced species of the TRX of *Ehrlichia chaffeensis* [78].

3.2. Backbone dynamics of TRX m

Backbone ^{15}N relaxation parameters were obtained for 78 residues (Fig. 4) out of the 100 residues (all amino acids, except the N-terminal one and the 7 prolines). The R_1 values were relatively uniform through all the sequence with a mean of 3.37 s^{-1} and a standard deviation of 0.27 s^{-1} (Fig. 4 A), excluding the first and last four residues in the sequence.

Conversely, the R_2 values showed a larger variation, with a mean of 7.18 s^{-1} and a standard deviation of 1.78 s^{-1}, excluding the first and last four residues in the sequence. The residues with the largest R_2 values ($\geq$ 8 s^{-1}) were: Cys33, Ile39 and Ala 40 (all of them involved or close to the active site); Ile54, Lys58, Leu59, Asn60 and Thr61 (all of them at the C terminus of β-strand 3); and Ala94, Val95 and Leu100 (all of them located in the loop following β-strand 5 and at the N terminus of α4). The large values of the R_2 in those residues indicate a high conformational exchange (i.e., in the microsecond-to-millisecond time regime) contribution [53].

The NOE values for residues involved in the elements of the secondary structure were not far from the theoretical one of 0.82, expected for an amide proton in a rigid environment at this field strength [53]. Smaller NOE ratios were observed at the N and C-terminal residues forming the elements of secondary structure as well as in many of the residues belonging to the regions connecting those elements of the secondary structure. For instance, the region preceding α4 had smaller NOE values (and it also showed the largest R_2 values, see above). Furthermore, residues belonging to the active site also had smaller NOE ratios than the rest of amino acids. Apart from the N terminus of the protein, the residues with the lowest NOE values (< 0.3) were: Ile18 (at the C terminus of α1) and Leu59 (at the end of β-strand 3).

An estimation of the correlation time of 2.1 $\pm$ 0.5 ns was obtained from a trimmed, averaged R_2/R_1 (excluding the last first and four terminal residues and those described above with large R_2 values). This value is smaller than that expected theoretically, for a 108-residue long protein, which should be ~4.3 ns [53]. Another examples of proteins with highly dynamic regions leading to anomalous estimations of the

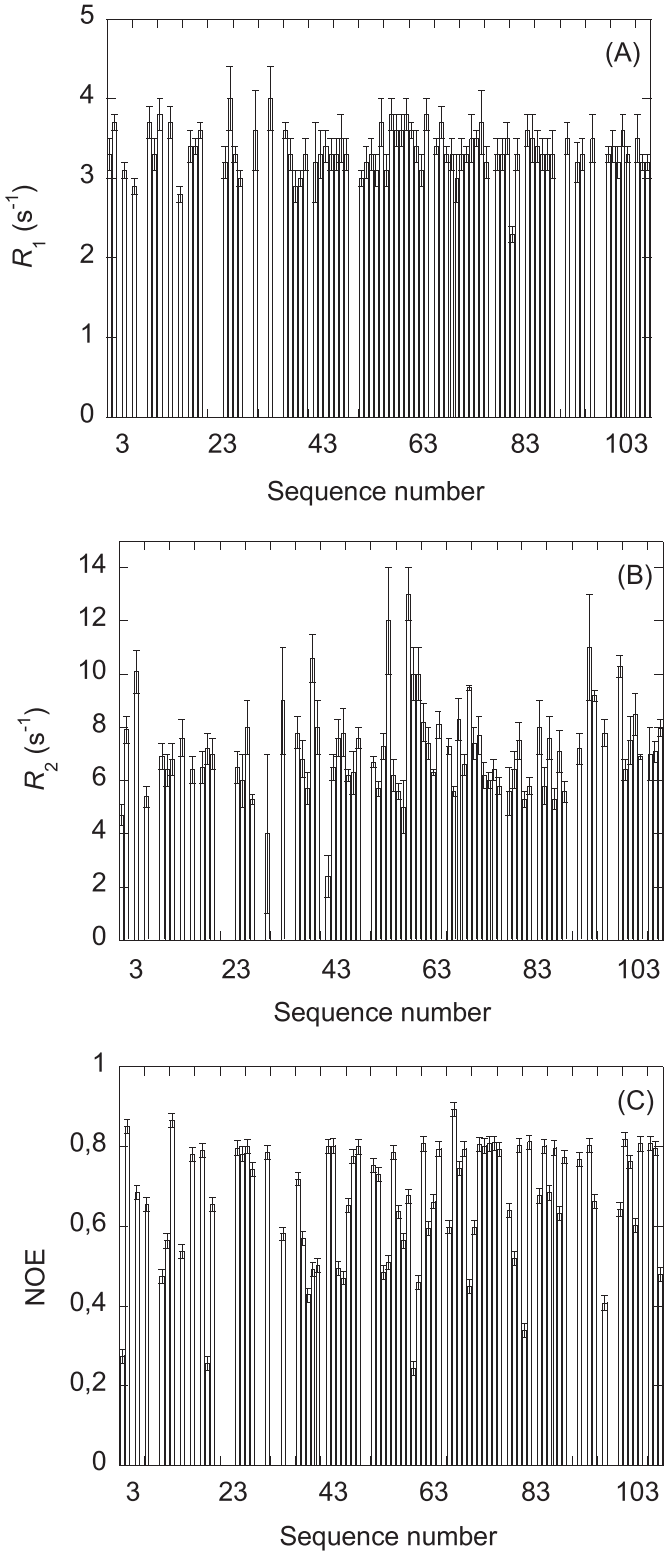

Fig. 4. Relaxation parameters of TRX m. The R_1 (A), R_2 (B) and NOE (C) values for residues of TRX m acquired at 500 MHz (11.14 T). Error bars in R_1 and R_2 are from fitting to exponential curves. Errors in NOE are estimated to be 10 % of the reported value.

correlation times, when compared to the theoretical ones, have been described in the literature [80,81]. In fact, it has been argued that the presence of nonterminal residues with a small R_2/R_1 ratio suggests the presence of two internal motions on different time scales [82–84].

3.3. Conformational preferences and binding to TRX m of the FBPpep

Before studying the binding of FBPpep to TRX m of pea, we studied its conformational preferences in isolation, by using two different spectroscopic techniques.

3.3.1. The isolated FBPpep was mainly disordered

We used far-UV CD to elucidate whether there was some secondary structure in the isolated peptide. The spectrum of the peptide showed an intense minimum at ~202 nm (Fig. S2), indicating that it acquired mostly a random-coil conformation. The spectrum also showed a small shoulder at 222 nm, which could be attributed to the presence of the sole aromatic residue in the sequence, Tyr157 [85–87]. In fact, fluorescence spectra of isolated FBPpep showed a maximum wavelength at 308 nm, which is characteristic of polypeptides containing a fluorescent tyrosine residue (data not shown).

We assigned FBPpep by using 2D ^{1}H NMR sequential assignment methods (Table ST2). Several lines of evidence from the analyses of 2D ^{1}H NMR spectra further confirmed the disordered nature of FBPpep in isolation in aqueous solution. First, the conformational shifts ($\Delta\delta$) of H_α protons [62–64] for all the assigned residues were within the commonly accepted range for random-coil peptides ($\Delta\delta \leq 0.1$ ppm) (Table ST2). Second, no long- or medium-range NOEs were detected, but only sequential ones (i.e. αN (i, i + 1) and βN (i, i + 1)) (Fig. 5). However, at the second half of FBPpep (residues Thr165 to Gln179) there was evidence of weak, sequential contacts between the amide protons of some residues, namely Asn164-Thr165, Gly167-Thr168, Thr168-Glu169, Val175-Asn176, Val177-Ser178 (for which all their H_α protons had $\Delta\delta \leq 0.1$ ppm, Fig. 5). And third, the temperature coefficients of the amide protons, which measure their solvent-accessibility, were in all residues in the range of −6.0 to −9.0 ppb K^{-1} (Table ST2), which are typical of solvent-exposed amide protons [65–67]; thus, all the amide protons of FBPpep were not hydrogen-bonded. A similar conclusion was reached when FBPpep was dissolved in D_2O and acquisition of a 1D ^{1}H NMR spectrum was carried out: no amide proton was observed after 5 min of dissolving the sample (data not shown).

3.3.2. Binding of FBPpep to TRX m

We measured the affinity of FBPpep in vitro for TRX m, by following a two-part experimental approach. First, we carried out a fluorescence titration to follow changes in the fluorescence of the protein upon peptide addition. And second, we carried out a 2D ^{1}H,^{15}N HSQC NMR titration to follow the changes in the intensity or in chemical shifts of the spectrum of TRX m as the peptide concentration was increased.

In the fluorescence experiments, there was a decrease in the fluorescence as the peptide concentration was raised. The value of the K_d for the binding reaction from these experiments was 1.7 ± 0.5 μM (Fig. 6 A); the fact that binding can be followed by excitation at 295 nm indicates that at least one of the tryptophan residues of TRX m (namely, Trp13, Trp29 or Trp32) was affected by peptide binding. On the other hand, in the NMR experiments, the intensity of all the signals decreased in a

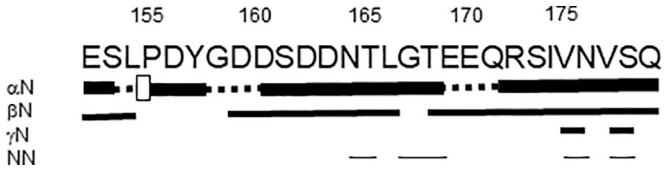

Fig. 5. NOE diagram of the FBPpep. NOEs are classified into strong, medium or weak, as represented by the height of the bar underneath the sequence; signal intensity was judged from the NOESY experiments by visual inspection. The dotted lines indicate NOE contacts that could not be unambiguously assigned due to overlapping with the chemical shifts of other nuclei. A white square indicates an αδ(i,i + 1) NOEs involving the Pro in the row corresponding to the αN NOEs.

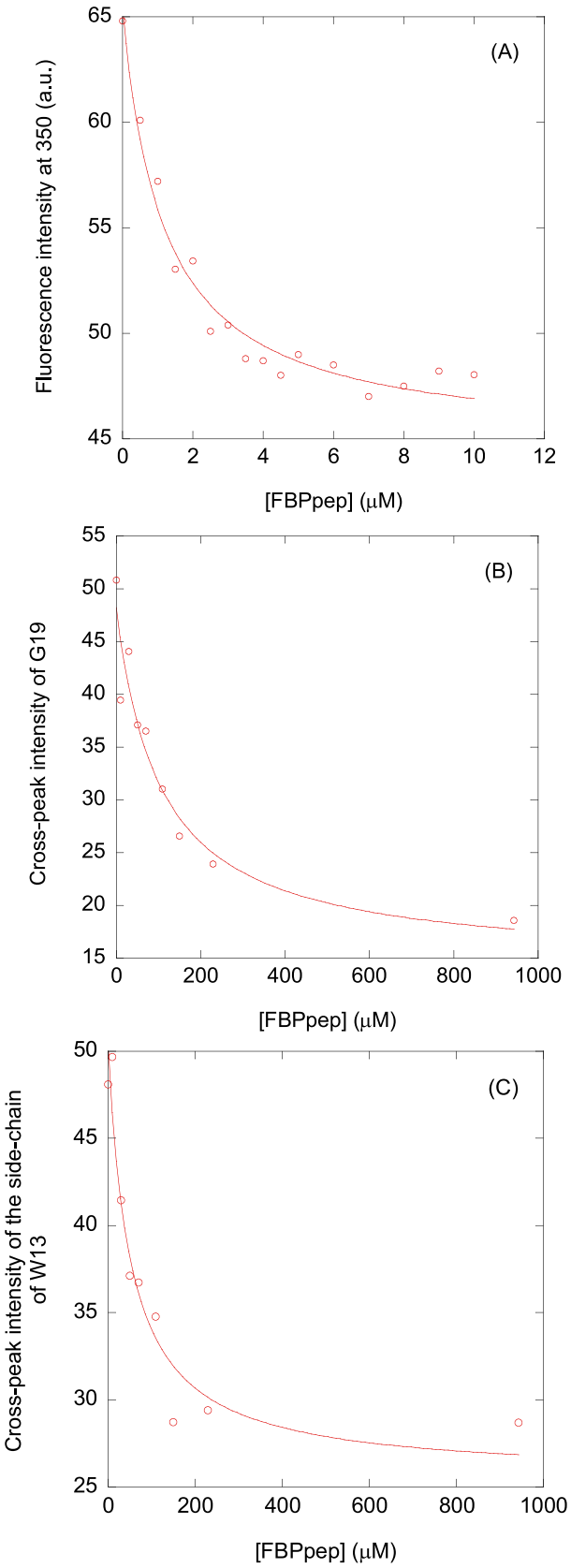

(caption on next column)

Fig. 6. Binding of FBPpep to TRX m as mapped by spectroscopic probes. (A) Titration curve obtained by monitoring the changes in the fluorescence at 315 nm when FBPpep was added to TRX m. The fluorescence intensity on the y-axis is the relative signal after removal of the corresponding blank. The line through the data is the fitting to Eq. (1). Experiments were carried out at 30 °C in phosphate buffer (50 mM), pH 5.8. The changes in the intensity of the backbone amide proton of Gly19 (B) and the indole chain of Trp13 (C) in the 2D $^{1}H,^{15}N$ HSQC NMR spectra upon addition of increasing concentrations of FBPpep. Experiments were carried out at 30 °C in phosphate buffer (50 mM), pH 5.8 in the presence of 1 mM DTT. The lines through the data of the intensities of the two selected cross-peaks are the corresponding fittings to Eq. (2).

sigmoidal way, as the FBPpep concentration was raised; furthermore, we did not observe any change in chemical shifts as the peptide concentration was increased. Furthermore, it seems there were no preferred regions in TRX m for peptide binding, or, alternatively, there was allosteric changes in all the molecule upon binding of the peptide. This general decrease in the intensity of all the signals precluded an unambiguous definition of the region of TRX m involved directly in peptide binding. Most of the sigmoidal variations of the cross-peaks intensities of TRX m could be fitted to Eq. (2), yielding similar K_d values, within the error. For instance, the K_d obtained from the intensity decrease in the cross-peak of the backbone amide proton of Gly19 was 104 ± 50 μM (Fig. 6 B), and that obtained from the variation of the cross-peak intensity of the indole side-chain of Trp13 was 52 ± 20 μM (Fig. 6 C). Although both values are similar within the error, the large fitting errors in the values from each cross-peak are probably due to: (i) the error in the intensities measured from the HSQC spectra (even after correcting for the values of the receiver gain); and, (ii) the absence of enough points where the binding curve is close to reach the saturation.

To sum up, both spectroscopic techniques unambiguously indicated that there was binding between TRX m and FBPpep, with a dissociation constant in the low micromolar range.

4. Discussion

4.1. Structure and dynamics of TRX m from pea

The solution structure of pea TRX m was similar to that of TRX m from spinach (which was also similar to the crystal structure of the same protein) [44]. However, one important difference with the structure of TRX m from spinach is that in this one, no NOE contacts were observed between β-strand 1 (residues 13 to 17) and β-strand 3 (residues 63 to 69) [44]; this absence of NOE contacts of β-strand 1 with the rest of the strands has also been observed in TRX h of *C. reinhardtii* [79]. Nevertheless, in the structure of TRX m from pea, NOE contacts were observed between the hydrogens involved in those strands (Fig. S1); for instance, we observed contacts between the NH of Lys58 and: (i) the side-chain of Val5; (ii) the amide proton of Val7 and the side-chain; and (iii) the H_α proton of Gln6, thus, pinpointing to the presence of this β-strand (Fig. S1).

Comparison with the solution structure of TRX m from spinach [44] showed two regions where the differences were more important. First, the active-site region and the following α2 appeared more separated from the rest of the molecule in the TRX m from pea, and the first turns of α2 did not appear to be well-formed (Fig. 2); in general terms, α2 and α4 appeared to be the less well-formed helices of TRX m from pea when compared to the similar helices of TRX m from spinach (Fig. 2). Furthermore, residues Cys33, Ile39 and Ala 40, at the N terminus of this helix, appeared to have a large flexibility as concluded from the large R_2 values (Fig. 4). And second, α4 in TRX m from pea appeared also more separated from the rest of the molecule at its N terminus and in a less parallel-like arrangement with α2 (Fig. 2) than in TRX m from spinach. In TRX m, we observed NOE contacts of the aromatic side-chain of Tyr50 (in α2) with the side-chains of Val104, Glu105 and Lys106 (all of them in α4), and we also detected NOEs of Ile42 with the side chain of Lys97;

that is, we observed NOEs with residues at the two termini of α2 with residues of α4. Interestingly enough, amino acids Ala94, Val95 and Leu100, at the N terminus of α4 had large R_2 values, indicating a high flexibility in the microsecond-to-millisecond time regime (Fig. 4 B). Taken together, these results suggest that the N-terminal of α4 in TRX m had a large flexibility and could move away from the rest of the protein. Movements of helical regions or of polypeptide patches nearby to them have been observed in: (a) a mutant of TRX of *Staphylococcus aureus*, involving a domain-swapping of the amino-terminal helix [88]; and (b) the wild-type PipX protein, where a helical region can adopt a flexed conformation in the free-target state of the protein involving residues with a high flexibility in the microsecond-to-millisecond time regime [89].

Another important difference with the TRX m from spinach is that the helical regions of TRX m from pea appeared more disordered and less regular. This could further support the hypothesis that TRX m from pea was more flexible. In fact, we observed that the picosecond-to-nanosecond dynamics of the pea protein showed for the amino acids involved in the elements of secondary structure NOE values close to the number expected for a residue in a rigid environment (0.82), but also the polypeptide patches in-between those regions showed NOE values very small, indicating a high flexibility (Fig. 4 C). Furthermore, residues around the active site, at both termini of β-strand 3, and at the N-terminal region of α4 showed a high mobility in the microsecond-to-millisecond time regime (i.e., high R_2 values). In addition, the fact that the trimmed, averaged R_2/R_1 yielded a lower correlation time value than that expected theoretically further supports the presence of several type of motions at different time scales for the amide protons [83,84]. Altogether, these findings suggest that the flexibility of pea TRX m was much larger than that of other members of the family. Although at this moment, we do not know the reasons behind such higher flexibility, it could be related to an improved ability to interact with a larger number of molecules, as it has been suggested in other small proteins such as PipX [89].

4.2. Binding of TRX m with the FBPpep

FBPase catalyzes the breakdown of fructose-1,6-bisphosphate to fructose-6-phosphate and inorganic phosphorous. FBPase activity is modulated by electron availability through the ferredoxin-thioredoxin system [26]: in fact, chloroplast FBPase can be activated by TRX f and TRX m [35,39,40,42]. It has been proposed that a long loop around residue 170 in FBPase is the region responsible for binding to either TRX f and TRX m [40]; this region contains a large amount of negatively charged residues (Asp and Glu), and appears partially disordered in the crystal structures of the FBPase from pea. Binding of the intact TRX m to FBPase, both from pea, resulted in a dissociation constant of 0.0188 μM (following a Koshland-Nemethy-Filmer model) [39]. In the case of spinach TRX f and FBPase, a K_d value of 800 nM has been reported for the non-covalent complex between the two proteins [90]. In this work, we wondered whether an isolated peptide derived from the interacting loop of FBPase could also bind to TRX m. Our results indicate that binding occurred with a dissociation constant in the range 1.3 (fluorescence)-50 μM (NMR); thus, there was binding between both molecules. At this stage, it is important to note that although NMR and fluorescence led to different values for the K_d, both of them are within the same range (low micromolar), and, those different values reflect the diverse range of protein concentrations employed in the experiments. The fact that the K_d was larger for FBPpep than for the intact FBPase indicates that, apart from the highly negatively charged loop region, other regions of FBP, and probably, its oligomeric state, are important in binding to TRX m (perhaps involving other hydrophobic interactions, as it has been suggested by protein engineering studies with the intact protein [40]). Furthermore, the lower affinity of the peptide for TRX m could indicate that since the peptide is disordered in isolation, as we have shown (Section 3.3.1), binding to TRX m also requires that the peptide acquires a native-like conformation as that in the intact FBPase. Then, our measurements (Fig. 6) would be reporting a folding-upon-binding event.

Residues Arg37, Lys70, Arg74 and Lys97 of TRX m have been shown to be important in binding to intact FBPase [37]. This region is also involved in binding to other monomer of the TRX h, where dimers of TRXs have been observed in crystal structures [91]. However, from the NMR titration, all the residues of pea TRX m were involved in binding (Figs. 6 B and C), since all of them had a sigmoidal-like behavior with dissociation constants within the same order of magnitude upon FBPpep addition. Thus, binding of FBPpep seemed to induce allosteric conformational changes through the whole molecule.

5. Conclusion

To sum up, we have solved the solution structure of thioredoxin m of *Pisum sativum*. The folding and arrangement of secondary structure elements are similar to those found in other thioredoxins m of other plants, but there seems to be a higher flexibility at the α-helix 4. Binding to a fragment of short of FBPase, containing the thioredoxin binding site, occurs with an affinity lower than that between the two intact proteins, suggesting that there are other factors, apart from the residues involved in the TRX-binding site, modulating the binding between the two intact TRX and FBPase proteins.

Funding and acknowledgements

This research was funded by Consellería de Innovación, Universidades, Ciencia y Sociedad Digital (Generalitat Valenciana) [CIAICO 2021/0135 to ACA and JLN]. The funders had no role in the study design, data collection and analysis, decision to publish, or preparation of the manuscript.

The authors thank people in the PDBe (Sudakshina Ganguly) for helpful suggestions and corrections on the structure deposition. We thank María Angeles Jiménez from Instituto de Química Física Blas Cabrera (CSIC) in Madrid for helpful discussions.

The authors thank the two anonymous reviewers for helpful suggestions and discussions. The authors thank Prof. Aichun Dong for handling the manuscript.

Deposition

The chemical shifts of TRX m from pea (^{13}C, ^{15}N and ^{1}H) have been deposited in the BMRB under the accession number 52150. The coordinates of the 20 conformers with the lowest target function have been deposited in the PDB, together with the list of restrictions (distances and angles) used, under the accession number 8QPD.

CRediT authorship contribution statement

José L. Neira: Writing – review & editing, Writing – original draft, Resources, Methodology, Investigation, Funding acquisition, Formal analysis, Conceptualization. **Martina Palomino-Schätzlein:** Writing – review & editing, Methodology, Investigation, Formal analysis. **Virginia Rejas:** Writing – review & editing, Investigation, Formal analysis. **José A. Traverso:** Writing – review & editing, Resources, Methodology, Investigation, Formal analysis. **Manual Rico:** Conceptualization. **Julio López-Gorgé:** Resources. **Ana Chueca:** Resources. **Ana Cámara-Artigas:** Writing – review & editing, Writing – original draft, Resources, Methodology, Investigation, Funding acquisition, Formal analysis, Conceptualization.

Declaration of competing interest

The authors declare that they have no known competing financial interests or personal relationships that could have appeared to influence

the work reported in this paper.

Data availability

The datasets generated during and/or analyzed during the current study are available from the corresponding authors on reasonable request.

Appendix A. Supplementary data

There are one figure describing the alignment of the β-strands in TRX m of pea and the observed NOEs (Fig. S1); the far-UV CD spectrum of isolated FBPpep (Fig. S2). Also, there are two tables containing the acquisition parameters of the full suite of acquired NMR spectra used to assign TRX m (Table ST1) and the ^{1}H assignment of FBPpep (Table ST2). Supplementary data to this article can be found online at https://doi.org/10.1016/j.ijbiomac.2024.129781.

References

[1] H. Eklund, F.K. Gleason, A. Holmgren, Structural and functional relations among thioredoxins of different species, Proteins 11 (1991) 13–28.
[2] H. Eklund, C. Cambillau, B.M. Sjöberg, A. Holmgren, H. Jörnvall, J.O. Höög, C. I. Brändén, Conformational and functional similarities between glutaredoxin and thioredoxins, EMBO J. 3 (1984) 1443–1449.
[3] A. Holmgren, M. Bjornstedt, Thioredoxin and thioredoxin reductase, Methods Enzymol. 252 (1995) 199–208.
[4] E.S.J. Arnér, A. Holmgren, Physiological functions of thioredoxin and thioredoxin reductase, Eur. J. Biochem. 267 (2000) 6102–6109.
[5] J.A. Traverso, F. Vignols, R. Cazalis, A. Pulido, M. Sahrawy, F.J. Cejudo, Y. Meyer, A. Chueca, PsTRXh1 and PsTRXh2 are both pea h-type thioredoxins with antagonistic behavior in redox imbalances, Plant Physiol. 143 (2007) 300–311.
[6] Y. Meyer, F. Vignols, J.P. Reichheld, Classification of plant thioredoxins by sequence similarity and intron position, Methods Enzymol. 347 (2002) 394–402.
[7] P. Stefankova, M. Kollarova, I. Barak, Thioredoxin-structural and functional complexity, Gen. Physiol. Biophys. 24 (2005) 3–11.
[8] M. Nishida, S. Harada, S. Noguchi, Y. Satow, H. Inoue, K. Takahashi, Three-dimensional structure of Escherichia coli glutathione S-transferase complexed with glutathione sulfonate: catalytic roles of Cys10 and His106, J. Mol. Biol. 281 (1998) 135–147.
[9] G. Tian, S. Xiang, R. Noiva, W.J. Lennarz, H. Schindelin, The crystal structure of yeast protein disulfide isomerase suggests cooperativity between its active sites, Cell 124 (2006) 61–73.
[10] J.L. Martin, J.C.A. Bardwell, J. Kuriyan, Crystal structure of the DsbA protein required for disulphide bond formation in vivo, Nature 365 (1993) 464–468.
[11] B.B. Buchanan, Y. Balmer, Redox regulation: a broadening horizon, Annu. Rev. Plant Biol. 56 (2005) 187–220.
[12] Y. Meyer, B.B. Buchanan, F. Vignols, J.P. Reichheld, Thioredoxins and glutaredoxins: unifying elements in redox biology, Annu. Rev. Genet. 43 (2009) 335–367.
[13] J.F. Collet, J. Messens, Structure, function, and mechanism of thioredoxin proteins, Antioxid. Redox Signal. 13 (2010) 1205–1216.
[14] Y. Meyer, C. Belin, V. Delorme-Hinoux, J.P. Reichheld, C. Riondet, Thioredoxin and glutaredoxin systems in plants: molecular mechanisms, crosstalks, and functional significance, Antioxid. Redox Signal. 17 (2012) 1124–1160.
[15] F. Montrichard, F. Alkhalfioui, H. Yano, W.H. Vensel, W.J. Hurkman, B. B. Buchanan, Thioredoxin targets in plants: the first 30 years, J. Proteome 72 (2009) 452–474.
[16] G. Powis, W.R. Montfort, Properties and biological activities of thioredoxins, Annu. Rev. Biophys. Biomol. Struct. 30 (2001) 421–455.
[17] M. Russel, P. Model, A. Holmgren, Thioredoxin or glutaredoxin in Escherichia coli is essential for sulfate reduction but not for deoxyribonucleotide synthesis, J. Bacteriol. 172 (1990) 1923–1929.
[18] J.R. Matthews, N. Wakasugi, J. Louis Virelizier, J. Yodoi, R.T. Hay, Thioredoxin regulates the DNA binding activity of NF-kappa B by reduction of a disulphide bond involving cysteine 62, Nucleic Acids Res. 20 (1992) 3821–3830.
[19] R. Scheibe, Redox-modulation of chloroplast enzymes : a common principle for individual control, Plant Physiol. 96 (1991) 1–3.
[20] J. Zhang, X. Li, X. Han, R. Liu, J. Fang, Targeting the thioredoxin system for cancer therapy, Trends Pharmacol. Sci. 38 (2017) 794–808.
[21] G. Bjørklund, L. Zou, M. Peana, C.T. Chasapis, T. Hangan, J. Lu, M. Maes, The role of the thioredoxin system in brain diseases, Antioxidants 11 (2022) 2161, https://doi.org/10.3390/antiox11112161.
[22] A. Burke-Gaffney, M.E.J. Callister, H. Nakamura, Thioredoxin: friend or foe in human disease? Trends Pharmacol. Sci. 26 (2005) 398–404.
[23] G. Spyrou, E. Enmark, A. Miranda-Vizuete, J.Å. Gustafsson, Cloning and expression of a novel mammalian thioredoxin, J. Biol. Chem. 272 (1997) 2936–2941.
[24] A. Miranda-Vizuete, A.E. Damdimopoulos, J.Å. Gustafsson, G. Spyrou, Cloning, expression, and characterization of a novel Escherichia coli thioredoxin, J. Biol. Chem. 272 (1997) 30841–30847.
[25] F. Sevilla, M.C. Martí, S. De Brasi-Velasco, A. Jiménez, Redox regulation, thioredoxins and glutaredoxins in retrograde signalling and in gene transcription, J. Exp. Bot. 74 (2023) 5955–5969, https://doi.org/10.1093/jxb/erad270.
[26] P. Schürmann, Ferredoxin: thioredoxin system, Methods Enzymol. 252 (1995) 274–283.
[27] L. Nikkanen, E. Rintamäki, Chloroplast thioredoxin systems dynamically regulate photosynthesis in plants, Biochem. J. 476 (2019) 1159–1172.
[28] B.B. Buchanan, The path to thioredoxin and redox regulation in chloroplasts, Annu. Rev. Plant Biol. 67 (2016) 1–24.
[29] E. Gelhaye, N. Rouhier, N. Navrot, J.P. Jacquot, The plant thioredoxin system, Cell. Mol. Life Sci. 62 (2005) 24–35.
[30] P. Geigenberger, I. Thormählen, D.M. Daloso, A.R. Fernie, The unprecedented versatility of the plant thioredoxin system, Trends Plant Sci. 22 (2017) 249–262.
[31] L. Nikkanen, J. Toivola, M.G. Diaz, E. Rintamäki, Chloroplast thioredoxin systems: prospects for improving photosynthesis, Philos. Trans. R. Soc. Lond. Ser. B Biol. Sci. 372 (2017).
[32] A.J. Serrato, J. Fernández-Trijueque, J. de D. Barajas-López, A. Chueca, M. Sahrawy, Plastid thioredoxins: a "one-for-all" redox-signaling system in plants, Front. Plant Sci. 4 (2013) 463, https://doi.org/10.3389/fpls.2013.00463.
[33] B.B. Buchanan, Regulation of CO2 assimilation in oxygenic photosynthesis: the ferredoxin/thioredoxin system. Perspective on its discovery, present status, and future development, Arch. Biochem. Biophys. 288 (1991) 1–9.
[34] P. Schürmann, K. Maeda, A. Tsugita, Isomers in thioredoxins of spinach chloroplasts, Eur. J. Biochem. 116 (1981) 37–45.
[35] I. Häberlein, B. Vogeler, Completion of the thioredoxin reaction mechanism: kinetic evidence for protein complexes between thioredoxin and fructose 1,6-bisphosphatase, Biochim. Biophys. Acta 1253 (1995) 169–174.
[36] M.K. Geck, F.W. Larimer, F.C. Hartman, Identification of residues of spinach thioredoxin f that influence interactions with target enzymes, J. Biol. Chem. 271 (1996) 24736–24740.
[37] J.L. Jaramillo, A. Chueca, J.P. Jacquot, R. Hermoso, J.J. Lázaro, M. Sahrawy, J. L. Gorgé, High-yield expression of pea thioredoxin m and assessment of its efficiency in chloroplast fructose-1,6-bisphosphatase activation, Plant Physiol. 114 (1997) 1169–1175.
[38] M. Sahrawy, A. Chueca, R. Hermoso, J.J. Lázaro, J. López Gorgé, Directed mutagenesis shows that the preceding region of the chloroplast fructose-1,6-bisphosphatase regulatory sequence is the thioredoxin docking site, J. Mol. Biol. 269 (1997) 623–630.
[39] O.S. Wangensteen, A. Chueca, M. Hirasawa, M. Sahrawy, D.B. Knaff, J. López Gorgé, Binding features of chloroplast fructose-1,6-bisphosphatase-thioredoxin interaction, Biochim. Biophys. Acta 1547 (2001) 156–166.
[40] A. Chueca, M. Sahrawy, E.A. Pagano, J. López Gorgé, Chloroplast fructose-1,6-bisphosphatase: structure and function, Photosynth. Res. 74 (2002) 235–249.
[41] Z. Liu, Antioxidant activity of the thioredoxin system, Biophys Rep. 9 (2023) 22–28.
[42] A. Reche, J. Jose Lazaro, R. Hermoso, A. Chueca, J. Lopez Gorge Reche, A. Reche, J.J. Lazaro, R. Hermoso, A. Chueca, J. Lopez Gorge, Binding and activation of pea chloroplast fructose-1,6-bisphosphatase by homologous thioredoxins m and f, Physiol. Plant. 101 (1997) 463–470.
[43] R. Hermoso, M. Castillo, A. Chueca, J.J. Lazaro, M. Sahrawy, J.L. Gorge, Binding site on pea chloroplast fructose-1,6-bisphosphatase involved in the interaction with thiore- doxin, Plant Mol. Biol. 30 (1996) 455–465.
[44] J.L. Neira, C. González, C. Toiron, G. De Prat-Gay, M. Rico, Three-dimensional solution structure and stability of thioredoxin m from spinach, Biochemistry 40 (2001) 15246–15256.
[45] D. Aguado-Llera, A.I. Martínez-Gómez, J. Prieto, M. Marenchino, J.A. Traverso, J. Gómez, A. Chueca, J.L. Neira, The conformational stability and biophysical properties of the eukaryotic thioredoxins of Pisum sativum are not family-conserved, PLoS One 6 (2011).
[46] J.L. Neira, M. Palomino-Schätzlein, E. Hurtado-Gómez, M.G. Ortore, A. Falcó, An N-terminal half fragment of the histidine phosphocarrier protein, HPr, is disordered but binds to HPr partners and shows antibacterial properties, Biochim. Biophys. Acta Gen. Subj. 1865 (2021).
[47] S.C. Gill, P.H. von Hippel, Calculation of protein extinction coefficients from amino acid sequence data, Anal. Biochem. 182 (1989) 319–326.
[48] M. Chiadmi, A. Navaza, M. Miginiac-Maslow, J.P. Jacquot, J. Cherfils, Redox signalling in the chloroplast: structure of oxidized pea fructose-1,6-bisphosphate phosphatase, EMBO J. 18 (1999) 6809–6815.
[49] J.P. Jacquot, J. Lopez-Jaramillo, M. Miginiac-Maslow, S. Lemaire, J. Cherfils, A. Chueca, J. Lopez-Gorge, Cysteine-153 is required for redox regulation of pea chloroplast fructose-1,6-bisphosphatase, FEBS Lett. 401 (1997) 143–147.
[50] B. Birdsall, R.W. King, M.R. Wheeler, C.A. Lewis, S.R. Goode, R.B. Dunlap, G.C. K. Roberts, Correction for light absorption in fluorescence studies of protein-ligand interactions, Anal. Biochem. 132 (1983) 353–361.
[51] D. Beckett, Measurement and analysis of equilibrium binding titrations: a beginner's guide, Methods Enzymol. 488 (2011) 1–16.
[52] C.A. Royer, S.F. Scarlata, Fluorescence approaches to quantifying biomolecular interactions, Methods Enzymol. 450 (2008) 79–106.
[53] J. Cavanagh, W.J. Fairbrother, A.G. Palmer, N.J. Skelton, Protein NMR Spectroscopy: Principles and Practice (2nd Edition), 2007.
[54] D. Pantoja-Uceda, J. Santoro, Amino acid type identification in NMR spectra of proteins via beta- and gamma-carbon edited experiments, J. Magn. Reson. 195 (2008) 187–195.
[55] D. Pantoja-Uceda, J. Santoro, New amino acid residue type identification experiments valid for protonated and deuterated proteins, J. Biomol. NMR 54 (2012) 145–153.

[56] N.A. Farrow, R. Muhandiram, S.M. Pascal, L.E. Kay, A.U. Singer, J.D. Forman-Kay, C.M. Kay, G. Gish, T. Pawson, S.E. Shoelson, Backbone dynamics of a free and phosphopeptide-complexed Src homology 2 domain studied by 15N NMR relaxation, Biochemistry 33 (1994) 5984–6003.
[57] Dominique Marion, Kurt Wüthrich, Application of phase sensitive two-dimensional correlated spectroscopy (COSY) for measurements of (1)H-(1)H spin-spin coupling constants in proteins. 1983, Biochem. Biophys. Res. Commun. 425 (2012) 519–526.
[58] A. Bax, D.G. Davis, MLEV-17-based two-dimensional homonuclear magnetization transfer spectroscopy, Journal of Magnetic Resonance (1969) 65 (1985) 355–360.
[59] A. Kumar, R.R. Ernst, K. Wüthrich, A two-dimensional nuclear Overhauser enhancement (2D NOE) experiment for the elucidation of complete proton-proton cross-relaxation networks in biological macromolecules, Biochem. Biophys. Res. Commun. 95 (1980) 1–6.
[60] J. Cavanagh, M. Rance, Suppression of cross-relaxation effects in TOCSY spectra via a modified DIPSI-2 mixing sequence, Journal of Magnetic Resonance (1969) 96 (1992) 670–678.
[61] M. Piotto, V. Saudek, V. Sklenář, Gradient-tailored excitation for single-quantum NMR spectroscopy of aqueous solutions, J. Biomol. NMR 2 (1992) 661–665.
[62] M. Kjaergaard, F.M. Poulsen, Sequence correction of random coil chemical shifts: correlation between neighbor correction factors and changes in the Ramachandran distribu- tion, J. Biomol. NMR 50 (2011) 157–165.
[63] M. Kjaergaard, S. Brander, F.M. Poulsen, Random coil chemical shift for intrinsically disordered proteins: effects of temperature and pH, J. Biomol. NMR 49 (2011) 139–149.
[64] S. Schwarzinger, G.J.A. Kroon, T.R. Foss, J. Chung, P.E. Wright, H.J. Dyson, Sequence-dependent correction of random coil NMR chemical shifts, J. Am. Chem. Soc. 123 (2001) 2970–2978.
[65] N.J. Baxter, M.P. Williamson, Temperature dependence of 1H chemical shifts in proteins, J. Biomol. NMR 9 (1997) 359–369.
[66] T. Cierpicki, I. Zhukov, R.A. Byrd, J. Otlewski, Hydrogen bonds in human ubiquitin reflected in temperature coefficients of amide protons, J. Magn. Reson. 157 (2002) 178–180.
[67] T. Cierpicki, J. Otlewski, Amide proton temperature coefficients as hydrogen bond indicators in proteins, J. Biomol. NMR 21 (2001) 249–261.
[68] G. Bodenhausen, D.J. Ruben, Natural abundance nitrogen-15 NMR by enhanced heteronuclear spectroscopy, Chem. Phys. Lett. 69 (1980) 185–189.
[69] W. Lee, M. Tonelli, J.L. Markley, NMRFAM-SPARKY: enhanced software for biomolecular NMR spectroscopy, Bioinformatics 31 (2015) 1325–1327.
[70] T. Herrmann, P. Güntert, K. Wüthrich, Protein NMR structure determination with automated NOE assignment using the new software CANDID and the torsion angle dynamics algorithm DYANA, J. Mol. Biol. 319 (2002) 209–227.
[71] P. Güntert, C. Mumenthaler, K. Wüthrich, Torsion angle dynamics for NMR structure calculation with the new program DYANA, J. Mol. Biol. 273 (1997) 283–298.
[72] P. Güntert, W. Braun, K. Wüthrich, Efficient computation of three-dimensional protein structures in solution from nuclear magnetic resonance data using the program DIANA and the supporting programs CALIBA, HABAS and GLOMSA. *J Mol Biol*. 217 (1991) 517–530.
[73] P. Güntert, Automated NMR structure calculation with CYANA, Methods Mol. Biol. 278 (2004) 353–378.
[74] P. Güntert, Automated NMR protein structure calculation, Prog. Nucl. Magn. Reson. Spectrosc. 43 (2003) 105–125.
[75] Y. Shen, F. Delaglio, G. Cornilescu, A. Bax, TALOS+: a hybrid method for predicting protein backbone torsion angles from NMR chemical shifts, J. Biomol. NMR 44 (2009) 213–223.
[76] P. Güntert, Calculating protein structures from NMR techniques, in: D.G. Reid (Ed.), Protein NMR Techniques, Methods in Molecular Biology, Humana Press INC, New Jersey, 1997, pp. 157–194.
[77] A. Bhattacharya, R. Tejero, G.T. Montelione, Evaluating protein structures determined by structural genomics consortia, Proteins 66 (2007) 778–795.
[78] G.W. Buchko, S.N. Hewitt, W.C. Van Voorhis, P.J. Myler, Solution NMR struc- tures of oxidized and reduced Ehrlichia chaffeensis thioredoxin: NMR-invisible structure owing to backbone dynamics, Acta Crystallogr F Struct Biol Commun. 74 (2018) 46–56.
[79] J.M. Lancelin, M. Stein, J.P. Jacquot, Secondary structure and protein folding of recombinant chloroplastic thioredoxin Ch2 from the green alga Chlamydomonas reinhardtii as determined by 1H NMR, J. Biochem. 114 (1993) 421–431.
[80] C.P.M. Van Mierlo, N.J. Darby, J. Keeler, D. Neuhaus, T.E. Creighton, Partially folded conformation of the (30-51) intermediate in the disulphide folding pathway of bovine pancreatic trypsin inhibitor. 1H and 15N resonance assignments and determination of backbone dynamics from 15N relaxation measurements, J. Mol. Biol. 229 (1993) 1125–1146.
[81] J.H. Viles, D. Donne, G. Kroon, S.B. Prusiner, F.E. Cohen, H.J. Dyson, P.E. Wright, Local structural plasticity of the prion protein, Analysis of NMR relaxation dynamics. Biochemistry. 40 (2001) 2743–2753.
[82] V.A. Jarymowycz, M.J. Stone, Fast time scale dynamics of protein backbones: NMR relaxation methods, applications, and functional consequences, Chem. Rev. 106 (2006) 1624–1671.
[83] G.M. Clore, P.C. Driscoll, A.M. Gronenborn, P.T. Wingfield, Analysis of the backbone dynamics of interleukin-1 beta using two-dimensional inverse detected hetero- nuclear 15N-1H NMR spectroscopy, Biochemistry 29 (1990) 7387–7401.
[84] M.D. Sørensen, S. Bjørn, K. Norris, O. Olsen, L. Petersen, T.L. James, J.J. Led, Solution structure and backbone dynamics of the human alpha3-chain type VI collagen C-terminal Kunitz domain, Biochemistry 36 (1997) 10439–10450.
[85] S. Vuilleumier, J. Sancho, R. Loewenthal, A.R. Fersht, Circular dichroism studies of barnase and its mutants: characterization of the contribution of aromatic side chains, Biochemistry 32 (1993) 10303–10313.
[86] S.M. Kelly, T.J. Jess, N.C. Price, How to study proteins by circular dichroism, Biochim. Biophys. Acta 1751 (2005) 119–139.
[87] A. Chakrabartty, T. Kortemme, S. Padmanabhan, R.L. Baldwin, Aromatic side-chain contribution to far-ultraviolet circular dichroism of helical peptides and its effect on measurement of helix propensities, Biochemistry 32 (1993) 5560–5565.
[88] A. Garcia-Pino, S. Martinez-Rodriguez, K. Wahni, L. Wyns, R. Loris, J. Messens, Coupling of domain swapping to kinetic stability in a thioredoxin mutant, J. Mol. Biol. 385 (2009) 1590–1599.
[89] A. Forcada-Nadal, M. Palomino-Schätzlein, J.L. Neira, A. Pineda-Lucena, V. Rubio, The PipX protein, when not bound to its targets, has its signaling C-terminal Helix in a flexed conformation, Biochemistry 56 (2017) 3211–3224.
[90] J.-M. Soulié, J. Buc, M. Riviére, J. Ricard, Equilibrium binding of thioredoxin fB to chloroplastic fructose bisphosphatase. Evidence for a thioredoxin site distinct from the active site, Eur. J. Biochem. 152 (1985) 565–568.
[91] K. Maeda, P. Hägglund, C. Finnie, B. Svensson, A. Henriksen, Crystal structures of barley thioredoxin h isoforms HvTrxh1 and HvTrxh2 reveal features involved in protein recognition and possibly in discriminating the isoform specificity, Protein Sci. 17 (2008) 1015–1024.